iScience

CellPress
OPEN ACCESS

Article

Satisfactory degradation of tetracycline by a pH-universal CoFe-LDH/MoS_2 heterojunction catalyst in Fenton process

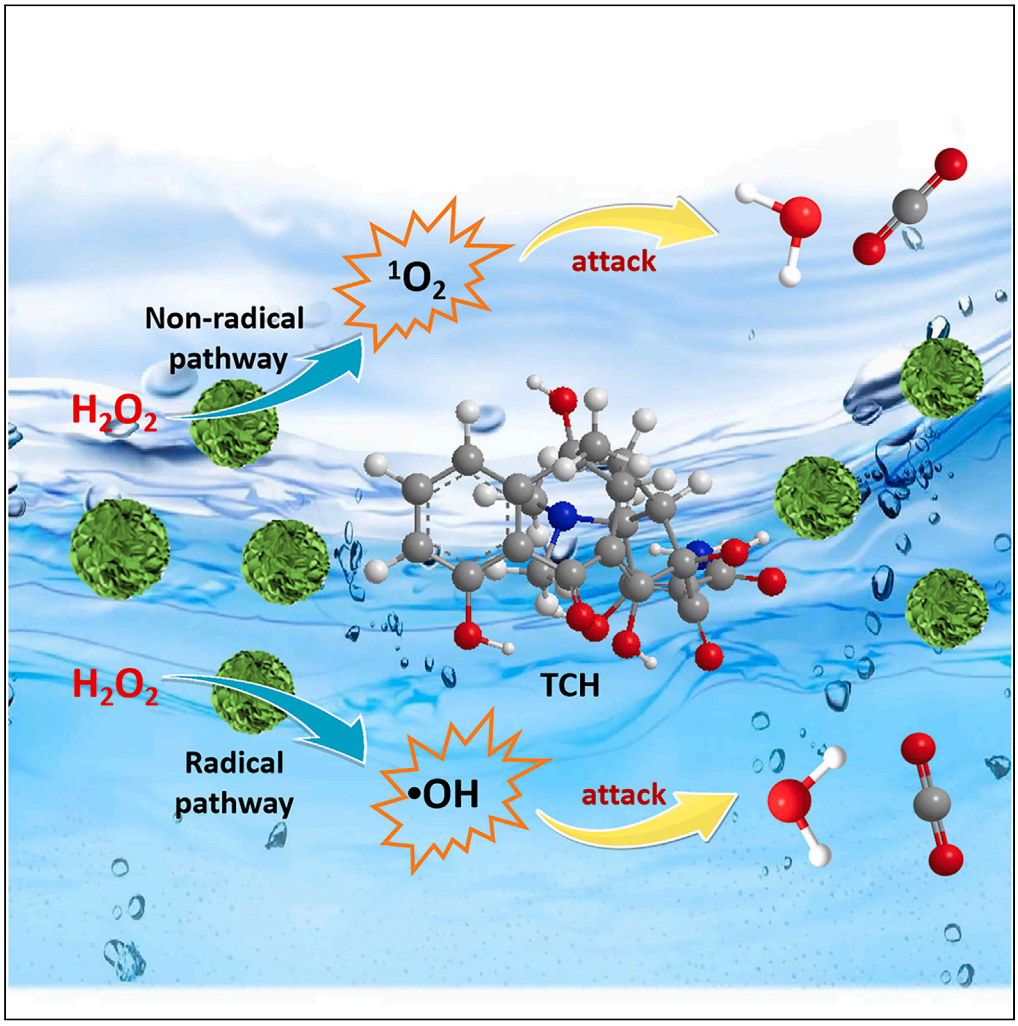

Meng Wang, Xiaoyu Li, Yanrui Su, ..., Faying Fan, Yufei Zhao, Wa Gao

zhaoyufei@mail.buct.edu.cn (Y.Z.)
gaowa@bua.edu.cn (W.G.)

Highlights

CoFe-LDH/MoS_2 catalyst was synthesized via facile electrostatic interactions

CoFe-LDH/MoS_2 catalysts exhibited superior performance in the degradation of TCH

The heterojunction catalysts could maintain high efficiency even after 10 cycles

Wang et al., iScience 27, 108996
February 16, 2024
https://doi.org/10.1016/j.isci.2024.108996

iScience

CellPress
OPEN ACCESS

Article

Satisfactory degradation of tetracycline by a pH-universal CoFe-LDH/MoS_2 heterojunction catalyst in Fenton process

Meng Wang,[1,2] Xiaoyu Li,[1] Yanrui Su,[1] Jiaoge Wu,[1] Tian Sun,[1] Xuan Xu,[1] Faying Fan,[3] Yufei Zhao,[2,*] and Wa Gao[1,4,*]

SUMMARY

Fenton or Fenton-like reactions have been widely used in various fields, including solar energy conversion to generate hydroxyl radicals, environmental remediation, biology, and life science. However, the slow Fe^{3+}/Fe^{2+} cycle and narrow applicable pH range still present significant challenges. Here, a heterostructured CoFe-layered double hydroxide/MoS_2 nanocomposite (CoFe-LDH/MoS_2) was prepared via simple electrostatic interactions. The heterostructure establishes a robust interfacial contact, leading to an abundance of exposed Mo^{6+} sites. Consequently, the developed CoFe-LDH/MoS_2+H_2O_2 system exhibited superior performance in the degradation of tetracycline (>85%) within 60 min across a wide pH range from acidic to basic. Moreover, the CoFe-LDH/MoS_2 heterojunction catalysts exhibited exceptional resistance to common anions and efficiently degraded various organic pollutants. The mechanism study verified that the CoFe-LDH/MoS_2 had high efficiency in producing $^1O_2$ and ·OH to degrade various organic pollutants. The present study will serve as a foundation for creating efficient catalyst systems for related environmental remediation.

INTRODUCTION

Tetracycline hydrochloride (TCH), a broad-spectrum antibiotic, is extensively utilized in the medical, aquaculture industries and animal husbandry. Unfortunately, its complete metabolism or absorption remains unattainable, thereby posing carcinogenic and mutagenic threats to ecosystems through leaching from medical antibiotics as well as agricultural, forestry, animal husbandry, and fishery applications.[1–4] Research has indicated that TCH is widely present in aquatic environments, such as pig farm wastewater and surrounding groundwater, with antibiotic concentrations ranging from 19.9 to 416.4 μg/L. Additionally, hospital pharmaceutical wastewater contains high levels of TCH, reaching concentrations as high as 100–500 mg/L.[5,6] Due to its complex ring structure, it exhibits a high degree of resistance to biodegradation.[7] Although physical technologies such as adsorption and membrane filtration can effectively eliminate TCH, they merely transfer it to a different phase without degradation, potentially leading to secondary pollution and incurring substantial costs.[8–10] Therefore, the development of highly effective strategies for the remediation and treatment of TCH remains one of the major objectives of exploration.

Recently, advanced oxidation processes (AOPs) using Fenton catalysts have attracted significant attention due to their potent oxidizing capacity, environmental friendliness, and high chemical stability.[11–14] The Fenton process involves the reaction between Fe^{2+} and H_2O_2 to generate robust reactive oxygen species (ROS), such as hydroxyl radical (•OH), superoxide radical ($•O_2^-$), and singlet oxygen ($^1O_2$).[15] These species exhibit efficient degradation of various organic contaminants into small molecules with low or no toxicity through a rapid and non-selective mechanism.[16,17] Heterogeneous Fenton processes employing solid catalyst for the remediation of organic pollutants overcome the limitations associated with homogeneous Fenton processes that use ferric salts in an acidic environment (pH < 3), which lead to sludge formation, reduced utilization of H_2O_2, and increased costs. As is known, the rate-limiting step in the Fenton reaction is the conversion of Fe^{3+} to Fe^{2+}, which severely restricts the degradation rate and presents a multitude of challenges for practical applications.[15,17] However, Fe^{3+}/Fe^{2+} cycle suffers from the extremely slow dynamics in the conventional Fenton process. Therefore, there is an urgent need for strategies to address this issue.

Layered double hydroxides (LDHs), which are 2D nanomaterials characterized by brucite-like laminates, exhibit great potential as inorganic materials for efficient heterogeneous Fenton catalysis in the removal of organic dyes due to their unique structure, compositional

[1]Key Laboratory for Northern Urban Agriculture of Ministry of Agriculture and Rural Affairs, College of Bioscience and Resources Environment, Beijing University of Agriculture, Beijing 102206, China
[2]State Key Laboratory of Chemical Resource Engineering, Beijing University of Chemical Technology, Beijing 100029, China
[3]Qingdao Industrial Energy Storage Research Institute, Qingdao Institute of Bioenergy and Bioprocess Technology, Chinese Academy of Science, Qingdao, Shandong 266101, China
[4]Lead contact
*Correspondence: zhaoyufei@mail.buct.edu.cn (Y.Z.), gaowa@bua.edu.cn (W.G.)
https://doi.org/10.1016/j.isci.2024.108996

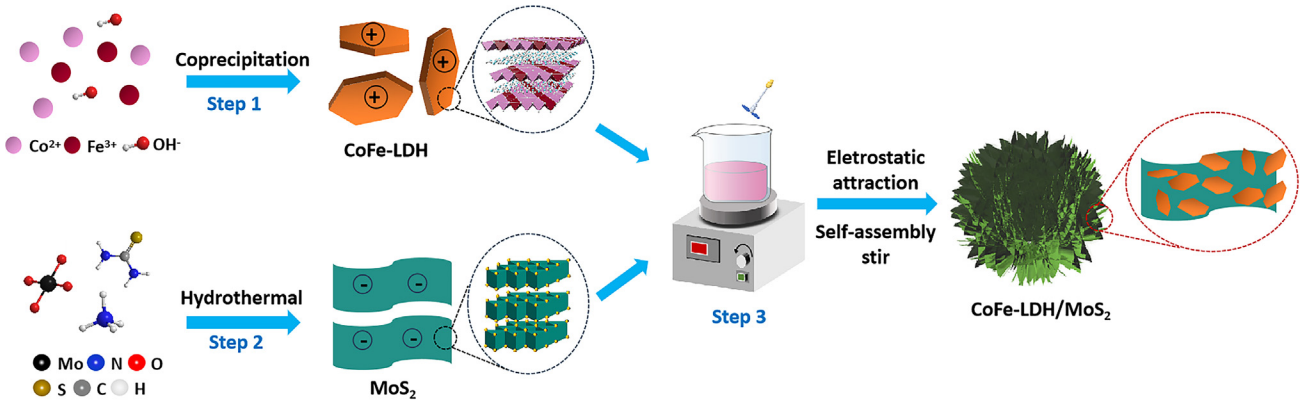

Figure 1. Schematic of the synthesis of CoFe-LDH, MoS_2, and CoFe-LDH/MoS_2 catalysts, respectively

versatility, ease of preparation, and cost-effectiveness.[15,18–21] Furthermore, the presence of hydroxyl groups on the sheets endows LDHs with highly hydrophilic properties, which facilitate the adsorption of hydrophilic contaminants and promote proximity between H_2O_2 molecules and active sites. This is crucial for driving the reaction. For example, Lu et al. employed CuZnFe-LDH/H_2O_2 to remove acetaminophen and arsenic pollutants in water, achieving complete degradation of acetaminophen within 24 h.[20] Zhang et al. shows that another important feature of LDH is that it may be composed of different divalent and trivalent metals, including Fe^{2+} and Fe^{3+}.[21] Nevertheless, there is still significant scope for enhancing the catalytic efficiency of Fe-containing LDHs by addressing the limited cycling of Fe^{3+}/Fe^{2+}, particularly in terms of improving the degree of mineralization. Transition metal sulfides (M_xS_y) are currently regarded as highly promising materials in the fields of biomedicine and wastewater treatment due to their diverse structures, variable valences, and limited solubility in aqueous solutions.[22,23] As a representative metal sulfide, molybdenum sulfide (MoS_2) has been identified as an efficient cocatalyst that significantly enhances the degradation efficiency of Fe^{2+}-catalyzed AOPs by facilitating the recycling rate of Fe^{3+}/Fe^{2+} through the Mo^{6+}/Mo^{4+} sites located at the edges of MoS_2 nanosheets.[22,24]

Herein, we have successfully developed a CoFe-LDH/MoS_2 heterojunction catalyst via simple electrostatic interactions. Experimental, HRTEM, XPS and EPR have effectively proven that the strong interface interaction of CoFe-LDH and MoS_2 can effectively promote Fe^{3+}/Fe^{2+} cycling and ensure rapid electron transfer, thereby facilitating the decomposition of H_2O_2 to generate a large amount of ROS through the built-in redox couple (Fe, Co, and Mo). As expected, the as-prepared CoFe-LDH/MoS_2 heterojunction catalysts exhibited robust performance in Fenton reaction across a wide pH range from acidic to basic for removing organic pollutants.

RESULTS AND DISCUSSION

Synthesis and morphology characteristics of CoFe-LDH/MoS_2

The synthesis procedure of catalysts was briefly summarized in the schematic diagram presented in Figure 1. After a facile hydrothermal treatment, co-precipitation process, self-assembly technique, and subsequent impurity removal steps, a successful integration of CoFe-LDH/MoS_2 heterojunction catalyst was achieved. As shown in Figure 2A, the X-ray diffraction (XRD) pattern of CoFe-LDH exhibited the characteristic set of (00*l*) peaks, which were consistent with the expected lamellar structure of LDH materials.[19] The diffraction peaks of MoS_2, which were observed at 2θ of 14.1°, 33.4°, 39.5°, and 59.2°, could be attributed to the crystallographic planes (002), (100), (103), and (110), respectively, in the 2H-MoS_2 phase (JCPDS card No. 37–1492).[23] Fortunately, the XRD characteristic peaks of CoFe-LDH and MoS_2 were simultaneously observed in the CoFe-LDH/MoS_2, indicating successful chemical compounding between CoFe-LDH and MoS_2. Additionally, Figure 2B presented the FTIR spectra of CoFe-LDH, MoS_2, and CoFe-LDH/MoS_2. The low-frequency band observed in the range of 500–900 cm^{-1} for CoFe-LDH corresponds to the lattice vibrations of metal-oxygen and metal-oxygen-metal bonds (Co–O, Fe–O, and Co–O–Fe). The peak at 1,384 cm^{-1} was attributed to the tensile vibration of the CO_3^{2-} anion. The absorption band at 3,600 cm^{-1} was assigned to the overlapping tensile vibration of the O–H group in CoFe-LDH. Furthermore, both the CO_3^{2-} anion and O–H tensile vibrations were observed in the CoFe-LDH/MoS_2 heterojunction catalyst. The Raman spectra of CoFe-LDH, MoS_2, and CoFe-LDH/MoS_2 catalyst were presented in Figure 2C. The peaks observed at 380.0 cm^{-1} and 405.2 cm^{-1} correspond to the in-plane vibrational mode (E_{2g}^1) and out-of-plane vibration mode (A_{1g}) of MoS_2, respectively.[25] In the CoFe-LDH/MoS_2 catalyst, simultaneous appearance of peaks at 380.0 cm^{-1} and 405.2 cm^{-1} was observed. Furthermore, the presence of peaks at 672 cm^{-1} and 890 cm^{-1} in CoFe-LDH/MoS_2 catalyst could be attributed to Mo-O bending vibration and Mo-*O*-Mo stretching vibrations in the octahedron,[26] respectively, providing further evidence for coordination between the two components in CoFe-LDH/MoS_2. These analyses provided compelling evidence for the successful synthesis of the CoFe-LDH/MoS_2 heterojunction catalyst.

The morphologies of the MoS_2, CoFe-LDH, and CoFe-LDH/MoS_2 were characterized using SEM and TEM imaging, as depicted in Figure 3. Pristine MoS_2 exhibited a hierarchical flower-like structure assembled by flakes, with nanoflowers having a diameter of approximately 200–500 nm (Figure 3A). The HRTEM image in Figure 3B revealed lattice fringes displaying interplanar spacings of 0.66 nm, which could be indexed

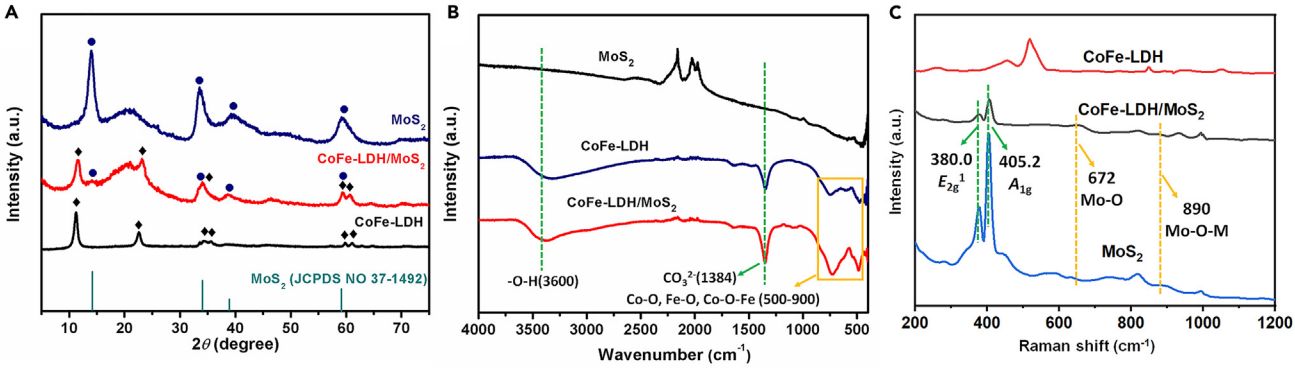

Figure 2. Structural characterization of the different catalysts

(A) XRD patterns of the MoS_2, CoFe-LDH, and CoFe-LDH/MoS_2 catalysts.

(B) FTIR spectra of the MoS_2, CoFe-LDH, and CoFe-LDH/MoS_2 catalysts.

(C) Raman spectra of the MoS_2, CoFe-LDH, and CoFe-LDH/MoS_2 catalysts.

as the (002) lattice plane of MoS_2.[23] Moreover, the HRTEM image (Figure 3C) revealed CoFe-LDH nanosheets of 50–80 nm with <5 nm thick, thereby exposing a greater number of active sites due to their ultrathin structure. After sufficient electrostatic interaction, it was clearly observed that the MoS_2 retained its original nanoflower morphology, whereas the LDH was uniformly dispersed within both the center and edge petals of the MoS_2 nanoflowers (Figures 3D and 3E). The presence of a heterojunction between CoFe-LDH and MoS_2 nanosheets was clearly observed in Figure 3F, where lattice fringes corresponding to the two precursors were seen in CoFe-LDH/MoS_2. The lattice fringes of 0.258 nm and 0.66 nm corresponded well with the (012) and (002) planes of the CoFe-LDH and MoS_2 precursors, respectively.[26] The TEM elemental mapping images of the CoFe-LDH/MoS_2 heterojunction catalyst in Figure 3G illustrated that the Co and Fe elements were uniformly distributed on the MoS_2, revealing the presence of CoFe-LDH on the surface of MoS_2. This promoted the formation of compact heterogeneous interfaces and enhanced charge transfer ability at the contact interface.

The specific surface area and pore volume of the samples were characterized by N_2 adsorption-desorption method. According to the calculations based on the BET equation, the specific surface areas of pure CoFe-LDH and CoFe-LDH/MoS_2 were determined as 93.29 m^2/g and 123.31 m^2/g, respectively. These results indicated that the incorporation of MoS_2 effectively prevented agglomeration of CoFe-LDH particles, resulting in a more uniform dispersion. Figure S1 exhibited a pore size distribution ranging from 2 to 10 nm for CoFe-LDH/MoS_2, indicating the presence of a mesoporous structure (2–50 nm) that offered abundant reaction sites and a substantial interfacial area. Moreover, CoFe-LDH/MoS_2 (Table S1) exhibited significantly higher pore volume (0.202555 cm^3/g) compared with CoFe-LDH (0.187827 cm^3/g). The above-mentioned results indicated that CoFe-LDH/MoS_2 heterojunction catalyst possessed an exceptional pore structure and a considerable surface area, which were favorable for the interaction between pollutants, catalysts, and H_2O_2 during the catalytic process.

Effects of different systems on TCH degradation

Firstly, adsorption experiments were conducted using CoFe-LDH, MoS_2, and CoFe-LDH/MoS_2 as adsorbents to investigate the removal of organic pollutants with TCH serving as the model pollutant. Figure S2 showed that MoS_2 exhibited a removal efficiency of 55.22% for TCH (100 mg/L) within a duration of 300 min, whereas CoFe-LDH demonstrated a slightly higher removal efficiency of 58.65% under the same conditions. The incorporation of CoFe-LDH/MoS_2 significantly enhanced the removal efficiency of TCH to an impressive rate of 60.91% within a shorter duration of 180 min, with the maximum adsorption capacity reaching 205.59 mg/g at an adsorbent dosage of 30 mg. The results demonstrated that the active adsorption sites became saturated as the TCH gradually adsorbed at this higher initial concentration, resulting in more TCH not to be adsorbed and retained in the solution. Therefore, the CoFe-LDH/MoS_2 could be employed as a heterogeneous catalyst for effectively removing TCH through Fenton-like reaction in the presence of H_2O_2. As depicted in Figure 4A, it was found that the degradation of TCH by CoFe-LDH and H_2O_2 alone was negligible, indicating their limited efficacy as catalysts. In the absence of H_2O_2, the CoFe-LDH/MoS_2 catalyst also exhibited a lack of TCH oxidation capability. These findings strongly suggest that chemical degradation serves as the primary mechanism for decontaminating TCH. When CoFe-LDH and MoS_2 were added simultaneously, representing the physical mixture (CoFe-LDH+MoS_2), the degradation efficiency of TCH was almost the same as CoFe-LDH alone. Interestingly, the removal efficiency of TCH was up to 94.1% in CoFe-LDH/MoS_2+H_2O_2 system, and H_2O_2 was nearly completely consumed after the reaction. Therefore, we inferred that the significant enhancement of the degradation efficiency observed in CoFe-LDH/MoS_2, as compared with the physical mixture, primarily originated from the formation of a heterojunction between CoFe-LDH and MoS_2. A pseudo-first-order kinetic model was used to calculate the rates of TCH degradation.[6]

$$\ln\left(\frac{C_t}{C_0}\right) = kt$$

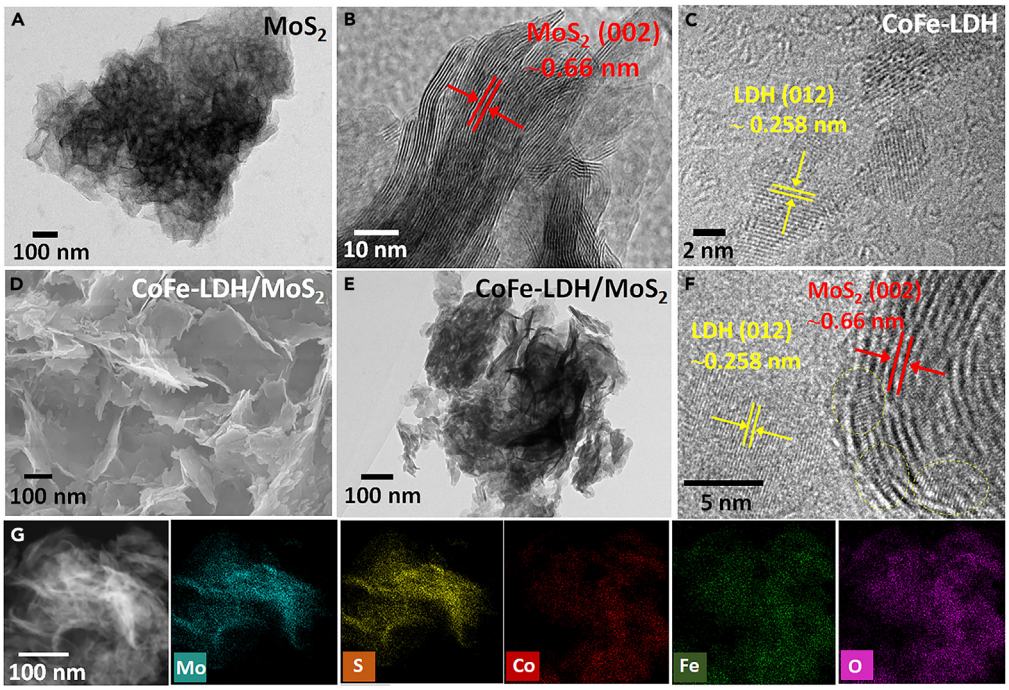

Figure 3. Morphology characterization of different catalysts

(A) TEM image of MoS_2.

(B) HRTEM image of MoS_2.

(C) HRTEM image of CoFe-LDH.

(D) SEM image of CoFe-LDH/MoS_2 catalyst.

(E) TEM image of CoFe-LDH/MoS_2 catalyst.

(F) HRTEM image of CoFe-LDH/MoS_2 catalyst.

(G) The elemental mapping of Mo, S, Co, Fe, and O of CoFe-LDH/MoS_2 catalyst.

where k is the TCH degradation rate, t is the reaction time, and C_0 and C_t stand for the TCH content at time 0 and t (min), respectively. The results presented in Figure 4B showed that the calculated k values for the H_2O_2, CoFe-LDH, CoFe-LDH/MoS_2, MoS_2+H_2O_2, CoFe-LDH+H_2O_2, CoFe-LDH+MoS_2+H_2O_2, and CoFe-LDH/MoS_2+H_2O_2 systems were 0.00143, 0.00301, 0.00287, 0.00534, 0.01952, 0.02356, and 0.03454 min^{-1}, respectively. Obviously, the abovementioned results further confirmed that the CoFe-LDH/MoS_2+H_2O_2 system had the best degradation performance for TCH.

It is well known that the bottleneck of Fenton reaction is the slow Fe^{3+}/Fe^{2+} cycle. To elucidate the role of MoS_2 in the Fenton reaction, we conducted TCH degradation experiments in a CoFe-LDH+H_2O_2 system with and without MoS_2. Figure S3 showed that the removal efficiency of TCH decreased rapidly from 93.6% to 32.1% in CoFe-LDH/MoS_2+H_2O_2 system as the ratio of MoS_2 decreased, indicating termination of reactions due to rapid exhaustion and slow regeneration of Fe^{2+}. Comparatively, the TCH removal efficiency in CoFe-LDH+H_2O_2 system was significantly lower at 75.5%, emphasizing the enhanced capability of MoS_2 to facilitate TCH degradation by efficiently activating H_2O_2 through an accelerated Fe^{3+}/Fe^{2+} cycle (Figure 4A). In addition, incorporating MoS_2 improved the dispersion of CoFe-LDH and increased exposure to catalytic sites for generating active species via H_2O_2 activation.

Effect of process conditions on catalytic reactions

The impact of key factors on the degradation of TCH was investigated. Figure 4C showed that the removal efficiency of TCH increased with an elevated dosage of CoFe-LDH/MoS_2 ranging from 10 to 50 mg/L, due to the enhanced availability of adsorption sites for TCH removal and catalytic sites for H_2O_2 activation facilitated by an increased quantity of CoFe-LDH/MoS_2. However, the treatment efficiency of TCH was almost unchanged when the dosage of CoFe-LDH/MoS_2 exceeded 30 mg/L, indicating that a dosage of 30 mg/L provided an adequate supply of catalytic sites. Considering the associated increase in treatment cost and risk of metal leakage with higher CoFe-LDH/MoS_2 dosages, 30 mg/L was determined as the optimal dosage. Figure 4D showed that the treatment rate decreased from 94.1% to 87.52% as the concentration of the TCH increased from 30 mg/L to 70 mg/L, resulting in a decrease in removal efficiency. This decline in removal efficiency was attributed to the limited availability of active species, which were unable to fully degrade TCH molecules present in the system, resulting in a slight decrease in degradation efficiency. However, it was noteworthy that even with an initial concentration of 30 mg/L, a removal efficiency of over 90% was still achieved within a span of 60 min.

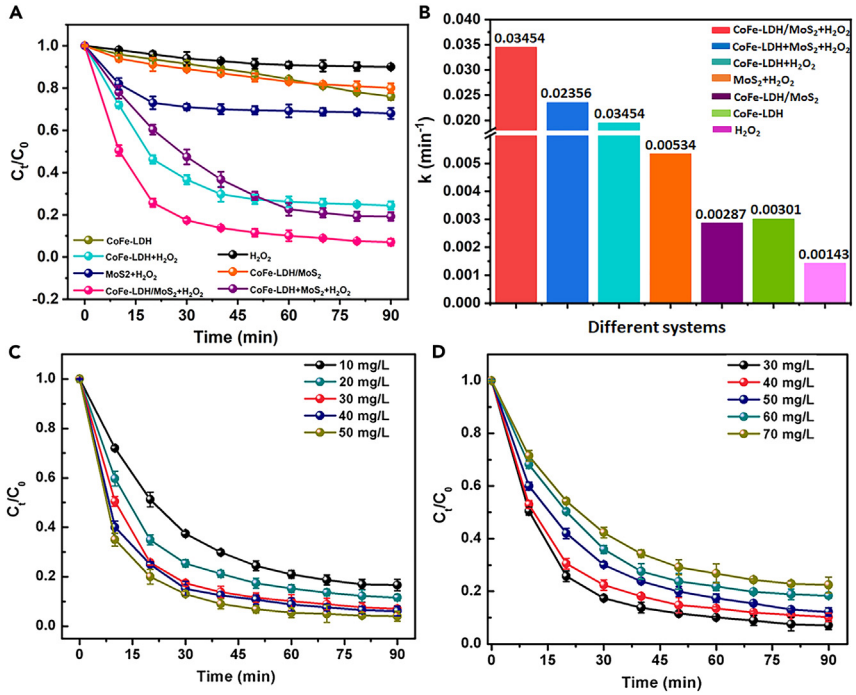

Figure 4. Effects of different systems on TCH degradation

(A) The degradation of the TCH under different catalyst systems.

(B) The corresponding degradation rate constant *k* under different catalyst systems.

(C) Effect of CoFe-LDHs/MoS_2 dosage on TCH degradation.

(D) Effect of TCH dosage on TCH degradation. Conditions: [TCH] = 30 mg/L, [Catalyst] = 30 mg/L, [H_2O_2] = 80 mmol/L, pH = 5.4, and T = 25 ± 2°C.

Narrow applicable pH range was another major bottleneck in Fenton reaction, even in the presence of MoS_2 as co-catalyst.[8,22] Therefore, an investigation was conducted to examine the effects of initial pH values on the CoFe-LDH/MoS_2-catalyzed Fenton reaction. To investigate the effect of initial pH on TCH degradation, the initial pH of the reaction solution was adjusted using 0.01 M HCl or NaOH prior to conducting the degradation experiment. Figure 5A demonstrated that over 85% of TCH could be rapidly eliminated across a wide pH range from 3.0 to 11.0. Such a broad pH window eliminated the need for traditional Fenton reactions' pH adjustment, providing significant advantages in terms of cost-effectiveness. In addition, considering the potential presence of variety co-existing substances in wastewater, Figure 5B illustrated the degradation statuses of TCH by CoFe-LDH/MoS_2 heterojunction catalyst under different anions conditions (Cl^-, NO_3^-, CO_3^{2-}, HCO_3^-, and $H_2PO_4^-$) with the same concentration of 10 mM. The inhibitory effect of these substances on TCH degradation was only marginal, as complete degradation of TCH could still be achieved within 90 min. The inhibiting effect of Cl^-, NO_3^-, CO_3^{2-}, HCO_3^-, and $H_2PO_4^-$ on TCH degradation was attributed to the quenching of the active radicals and subsequent formation of secondary radicals with lower activity that impede TCH oxidation.[27] From what has been discussed earlier, the CoFe-LDH/MoS_2+H_2O_2 system has obvious resistance to inorganic anions. Figure 5C further evaluated the performance of the CoFe-LDH/MoS_2+H_2O_2 system in degrading various organic pollutant. Notably, RhB, MO, and Phenol exhibited removal efficiencies of approximately 74.2%, 72.9%, and 84.9% within a span of 90 min, respectively. These results validated the effectiveness of the CoFe-LDH/MoS_2+H_2O_2 system in decomposing diverse organic pollutants, thereby highlighting its potential for practical applications.

Reusability and stability of CoFe-LDHs/MoS_2

The recyclability of the catalyst is a crucial factor for its industrial application. Cycling experiments were conducted to evaluate the stability of the CoFe-LDHs/MoS_2 heterojunction catalyst. As depicted in Figure 5D, even after 10 cycles, the efficiency degradation of TCH remained at 90.4%, slightly lower than the initial value. This slight decrease in TCH degradation can be attributed to both cobalt- and ion-leaching-induced loss of catalytic sites and adsorption of intermediates on the surface of CoFe-LDH/MoS_2 heterojunction catalyst.[28]

The leakage of total cobalt and iron ions during cycling was evaluated using ICP-OES, as depicted in Figure S4. Over 10 cycles, the system environment experienced minimal amounts of iron ions (<0.20 mg/L) and cobalt ions (<0.15 mg/L) leakage, which complied with China's Surface Water Environmental Quality Standards (GB3838-2002). According to previous reports, Fe^{2+} and Fe^{3+} can be colored by 1,10-phenanthroline and potassium thiocyanate (KSCN), respectively.[12] Therefore, dynamic simulations were conducted to monitor the fluctuations in Fe^{2+} and Fe^{3+} concentrations in both CoFe-LDH/MoS_2+H_2O_2 and CoFe-LDH+H_2O_2 systems throughout the reaction process. The results showed that the leaching of Fe^{2+} and Fe^{3+} concentrations remained below the detection limits of UV-vis spectrometer during the entire

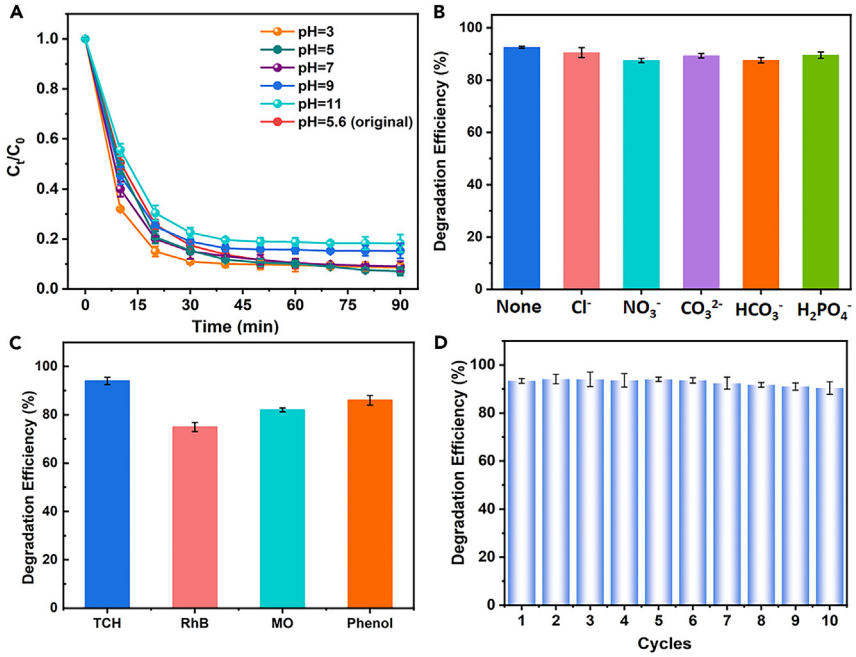

Figure 5. The effect of process conditions on the degradation of TCH by CoFe-LDH/MoS_2+H_2O_2 system

(A) Effects of initial pH.

(B) Effect of various typical anions.

(C) Removal of different kinds of organic pollutants, which were referred to TCH, RhB, MO and Phenol, respectively.

(D) Cycle test of CoFe-LDH/MoS_2, Conditions: [TCH] = 30 mg/L, [Catalyst] = 30 mg/L, [H_2O_2] = 80 mmol/L, pH = 5.4, and T = 25 ± 2°C.

course of the reaction, indicating excellent stability and reusability of CoFe-LDH-based catalysts. Additionally, Figure S5 showed that there was no obvious change in the characteristic peaks of XRD patterns of CoFe-LDH/MoS_2 after 10 cycles, further confirming the stability of CoFe-LDH/MoS_2. Importantly, it was noteworthy that the CoFe-LDH/MoS_2 synthesized in this study exhibited superior degradation of TCH compared with recent catalytic systems reported in Table S2.

Proposed reaction mechanisms of the catalytic CoFe-LDH/MoS_2+H_2O_2 process

Investigation of CoFe-LDH/MoS_2 interfacial effect

The chemical state changes of CoFe-LDH/MoS_2 were identified using XPS in order to investigate the underlying mechanism of H_2O_2 activation by CoFe-LDH/MoS_2. As shown in Figure S6, characteristic peaks corresponding to Fe 2p, Co 2p, O 1s, Mo 3d, and S 2p were observed for the prepared CoFe-LDH/MoS_2, which was consistent with the results obtained from TEM elemental mapping. The high-resolution Fe 2p XPS spectrum of CoFe-LDH exhibited five peaks (Figure 6A), including satellite peak at 718.53 eV. The peaks at 725.49 eV and 711.07 eV corresponded to Fe^{2+} 2p1/2 and Fe^{2+} 2p3/2, respectively, whereas those at 713.31 eV belonged to Fe^{3+} 2p3/2, respectively.[6,15,29] The relative surface content of $\equiv Fe^{2+}$ in CoFe-LDH increased upon compounding with MoS_2. It was noteworthy that the chemical combination with MoS_2 induced a shift in the Fe 2p XPS peak position of CoFe-LDH toward higher binding energy (713.31–714.05 eV), which could be attributed to electron transfer between MoS_2 and CoFe-LDH. This hypothesis was confirmed by the Mo 3d XPS spectra, as depicted in Figure 6B. The relative proportions of $\equiv Mo^{5+}$ (230.05 eV) and $\equiv Mo^{6+}$ (235.36 eV, 233.2 eV) on the surface of CoFe-LDH/MoS_2 showed a significant increase upon compounding with MoS_2, whereas the peak position of $\equiv Mo^{4+}$ (232.39 eV vs. 232.26 eV, 229.24 vs. 229.14 eV) shifted toward lower binding energy.[22,30] The presence of high-valent Mo indicated the occurrence of a redox reaction during the combination of CoFe-LDH and MoS_2. Due to the lower electronegativity of Fe compared with Mo, the Mo–O–Fe bonds resulted in an increased electron cloud density around $\equiv Mo^{4+}$. Furthermore, compared with MoS_2, a slight shift toward higher binding energy was observed for most of the S 2p peaks in CoFe-LDH/MoS_2 (Figure 6C), indicating the potential formation of Fe–S–Mo or Co–S–Mo bonds between CoFe-LDH and MoS_2.[30]

The spectrum of Co 2p in Figure 6D showed peaks corresponding to Co 2p3/2 (781.99 eV, 780.68 eV) and Co 2p1/2 (797.29 eV, 796.61 eV), along with two satellite peaks in the CoFe-LDH. The peaks at 781.99 and 796.61 eV could be attributed to $\equiv Co^{2+}$ and $\equiv Co^{3+}$ in octahedral sites, respectively.[1,31] Notably, the content of $\equiv Co^{3+}$ on the surface of CoFe-LDH significantly increased upon combination with MoS_2, indicating that the formation of Mo–S–Co bonds at the interface facilitated the generation of Co^{3+} on the surface of CoFe-LDH after forming a heterostructure with MoS_2. Through the aforementioned XPS analysis, we have confirmed the presence of Mo–O–Fe, Mo–S–Fe, or Mo–S–Co bonds at the interface between CoFe-LDH and MoS_2. These bonds played a crucial role in facilitating the establishment of Fe^{3+}/Fe^{2+} cycling on the catalyst surface. After the reaction (Figure 6E), the fraction of Fe^{3+} on the CoFe-LDH/MoS_2 surface decreased from 47.59% to 33.47%, whereas the fraction of

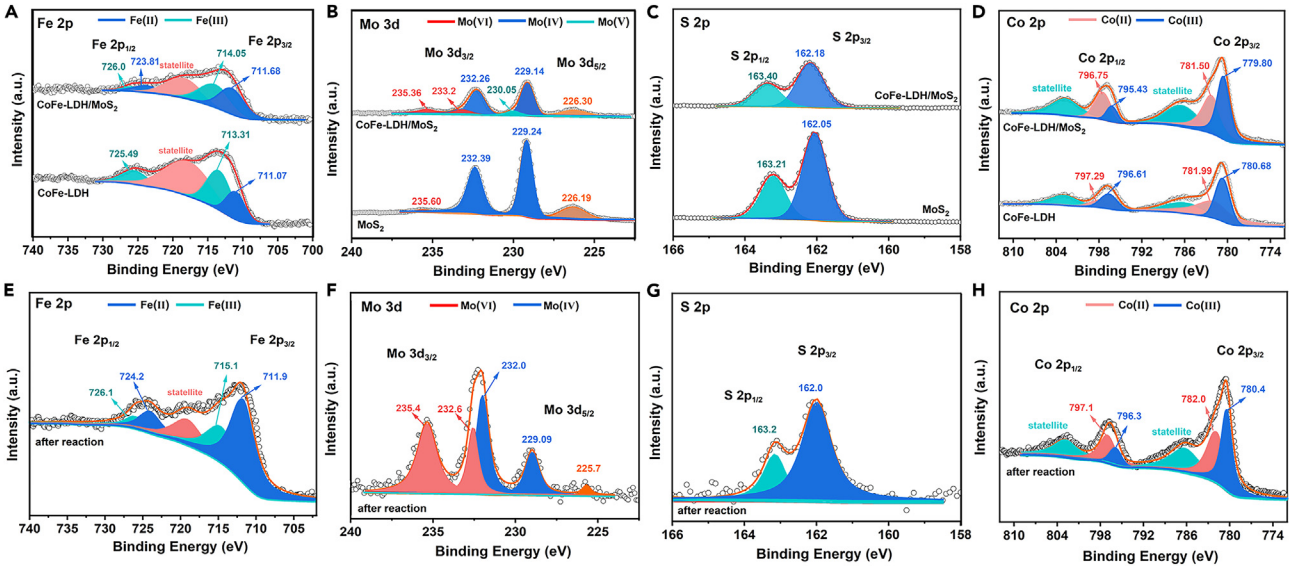

Figure 6. XPS spectra of CoFe-LDH/MoS_2 and used CoFe-LDH/MoS_2 catalyst

(A–D) (A) Fe 2p, (B) Mo 3d, (C) S 2p, (D) Co 2p scan of CoFe-LDH/MoS_2 catalyst.

(E–H) (E) Fe 2p, (F) Mo 3d, (G) S 2p, (H) Co 2p scan of used CoFe-LDH/MoS_2 catalyst.

Fe^{2+} increased from 52.40% to 66.52%. Moreover, the relative ratio of two Co 2p3/2 peaks corresponding to Co^{3+} and Co^{2+} shifted from 44.59% and 55.40% to 43.24% and 56.76%, respectively (Figure 6H). Additionally, Figure 6F demonstrated a reduction in the intensity of Mo^{4+} peaks (82.99%–46.76%) and an enhancement in the intensity of Mo^{6+} (17.01%–53.24%) pre- and post-reaction, accompanied by a slight shift in peak positions. This phenomenon can be attributed to the oxidation of partial Mo^{4+} to Mo^{6+}, concomitant with reduction of Fe^{3+} (Equations 1, 2, and 3). These XPS findings indicated that the Fe^{3+}/Fe^{2+} and Co^{2+}/Co^{3+} redox pair (Equations 9, 10, and 11) were realized by adding the MoS_2.

Identification of active species

To elucidate the possible mechanism of CoFe-LDH/MoS_2 catalytic process for TCH degradation, we conducted trapping tests using scavengers to detect the involved ROS. Specifically, *p*-benzoquinone (*p*-BQ), tert-butyl alcohol (TBA), and furfuryl alcohol (FFA) were introduced as quenching agents to scavenge of $\cdot O_2^-$, •OH, and $^1O_2$, respectively.[29] According to Figures 7A and S7, the addition of *p*-BQ at various concentrations did not significantly inhibit TCH removal, suggesting a slight effect of $\cdot O_2^-$. The introduction of different concentrations of TBA into the process resulted in a decrease in TCH degradation efficiency to 56.45%, primarily due to the elimination of •OH. However, the removal of TCH decreased significantly from 94.1% to 20.3% with the addition and increased concentration of FFA, thereby indicating that $^1O_2$ was the dominant ROS in the CoFe-LDH/MoS_2+H_2O_2 system.

Electron paramagnetic resonance (EPR) measurements, using 5,5-dimethyl-1-pyrrolidine-N-oxide (DMPO) and 2,2,6,6-tetramethyl-4-piperidone (TEMP) as the spin-trapping agents, further confirmed this conclusion.[15,32] Figure 7B showed that no DMPO-•OH signal peak was observed in the initial reaction stage in the H_2O_2+DMPO systems and MoS_2+H_2O_2+DMPO. However, a DMPO-•OH signal peak with a ratio of 1:2:2:1 was observed in the CoFe-LDH+H_2O_2+DMPO and CoFe-LDH/MoS_2+H_2O_2+DMPO, indicating that CoFe-LDH and CoFe-LDH/MoS_2 possess the ability to activate H_2O_2 to generate •OH (Equation 3). Besides, no DMPO-$\cdot O_2^-$ signal was detected in either the MoS_2+H_2O_2 or CoFe-LDH/MoS_2 system, providing further confirmation of the crucial role played by CoFe-LDH in enhancing degradation efficiency. Additionally, the presence of six weak characteristic signals for DMPO-$\cdot O_2^-$ in the CoFe-LDH+H_2O_2 and CoFe-LDH/MoS_2+H_2O_2 system suggested a lower possibility of radical-dominant oxidation (Figure 7C). Regarding the role of $^1O_2$, the generated $^1O_2$ from the CoFe-LDH+H_2O_2, MoS_2+H_2O_2 and CoFe-LDH/MoS_2+H_2O_2 system was effectively captured by TEMP (Figure 7D). The $^1O_2$ with an intensity ratio of 1:1:1 was observed in both CoFe-LDH+H_2O_2 and MoS_2+H_2O_2 systems[33]; however, these two radicals exhibited a higher intensity in the CoFe-LDH/MoS_2+H_2O_2 system, indicating that MoS_2 could promote pollutant removal through enhanced production of non-free radical $^1O_2$. Compared with •OH, $^1O_2$ has a longer lifetime. Consequently, in the presence of •OH, a fraction of it will react with $\cdot O_2^-$, leading to the consumption of a portion of the latter and subsequently enhancing the production of $^1O_2$ according to Equations 6 and 7. Previous research concluded that MoS_2 mixed with Fe^{2+} form a Fenton-like system capable of generating abundant $^1O_2$ and effectively degrading organic pollutants.[34,35] Therefore, eliminating both •OH and $\cdot O_2^-$ resulted in an increase in $^1O_2$ levels, which was more favorable for achieving long-term degradation of organic pollutants through Fenton or Fenton-like reactions.

In a heterogeneous Fenton reaction, the conversion rate of Fe^{3+} to Fe^{2+} is the rate-limiting step.[36] In our work, the co-catalytic effect of MoS_2 realized iron circulation on the surface of CoFe-LDH/MoS_2 (Equations 1, 2, 3, 4, 5, 6, 7, 8, 9, 10, and 11). The $\equiv Fe^{2+}$ on the catalyst surface decomposed H_2O_2 to generate •OH. However, due to the short lifetime and limited migration distance of •OH, it was easy to continue the

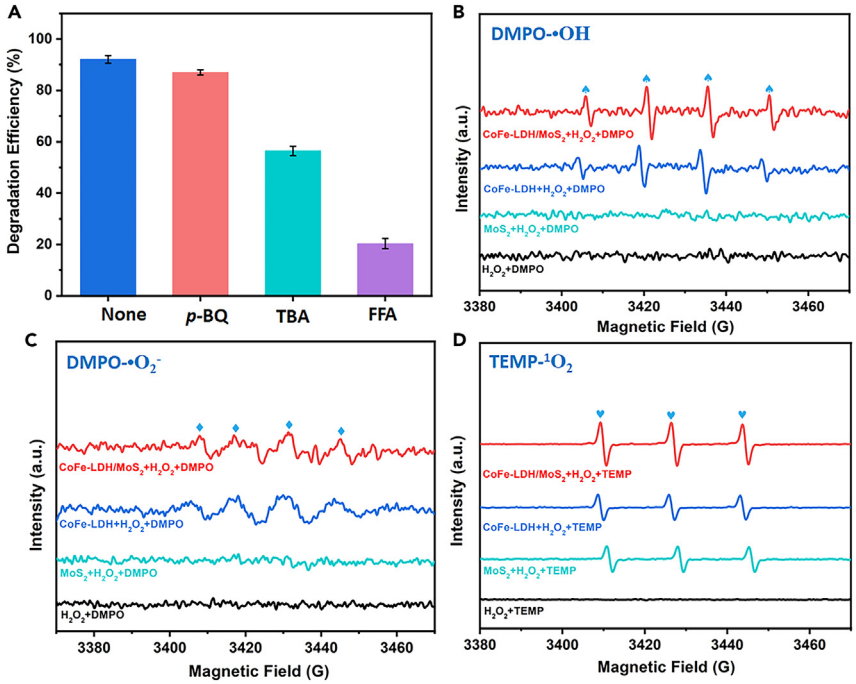

Figure 7. Investigation of the mechanism of CoFe-LDH/MoS_2+H_2O_2 system

(A) Scavenger quenching test. Conditions: [TCH] = 30 mg/L, [Catalyst] = 30 mg/L, [H_2O_2] = 80 mmol/L, pH = 5.4, and T = 25 ± 2°C.

(B) The EPR characterization in the different system using DMPO for identifying •OH.

(C) DMPO for identifying $\cdot O_2^-$.

(D) TEMP for identifying $^1O_2$.

reactions to generate $\cdot O_2^-$ and $^1O_2$, as shown in Equations 3, 4, 5, 6, 7, 8, and 11.[16,30] Moreover, the presence of $\equiv Co^{3+}$ and $\equiv Mo^{6+}$ on the surface of CoFe-LDH/MoS_2 further promoted the directional conversion of $\cdot O_2^-$ to $^1O_2$ (Equations 10 and 11).[30,36] Finally, the entire Fenton system was dominated by $^1O_2$ for efficient degradation of organic pollutants, facilitating H_2O_2 decomposition and generating a significant amount of ROS through the built-in redox couple (Fe, Co, and Mo).

$$\equiv Mo^{4+} + \equiv Fe^{3+} \rightarrow \equiv Mo^{6+} + \equiv Fe^{2+} \quad \text{(Equation 1)}$$

$$\equiv Mo^{6+} + H_2O_2 \rightarrow \equiv Mo^{4+} + H_2O + O_2 \quad \text{(Equation 2)}$$

$$\equiv Fe^{2+} + H_2O_2 \rightarrow \cdot OH + \equiv Fe^{3+} + OH^- \quad \text{(Equation 3)}$$

$$4 \cdot OH \rightarrow {}^1O_2 + 2H_2O \quad \text{(Equation 4)}$$

$$\cdot OH + H_2O_2 \rightarrow HO_2 \cdot + H_2O \quad \text{(Equation 5)}$$

$$HO_2 \cdot \rightarrow \cdot O_2^- + H^+ \quad \text{(Equation 6)}$$

$$2 \cdot O_2^- + 2H_2O \rightarrow {}^1O_2 + H_2O_2 + 2OH^- \quad \text{(Equation 7)}$$

$$\equiv Fe^{2+} + O_2 \rightarrow \equiv Fe^{3+} + \cdot O_2^- \quad \text{(Equation 8)}$$

$$\equiv Co^{2+} + H_2O_2 \rightarrow \equiv Co^{3+} + \cdot OH \quad \text{(Equation 9)}$$

$$\cdot O_2^- + \equiv Co^{3+} \rightarrow {}^1O_2 + \equiv Co^{2+} \quad \text{(Equation 10)}$$

$$\cdot O_2^- + \equiv Mo^{6+} \rightarrow {}^1O_2 + \equiv Mo^{4+} \quad \text{(Equation 11)}$$

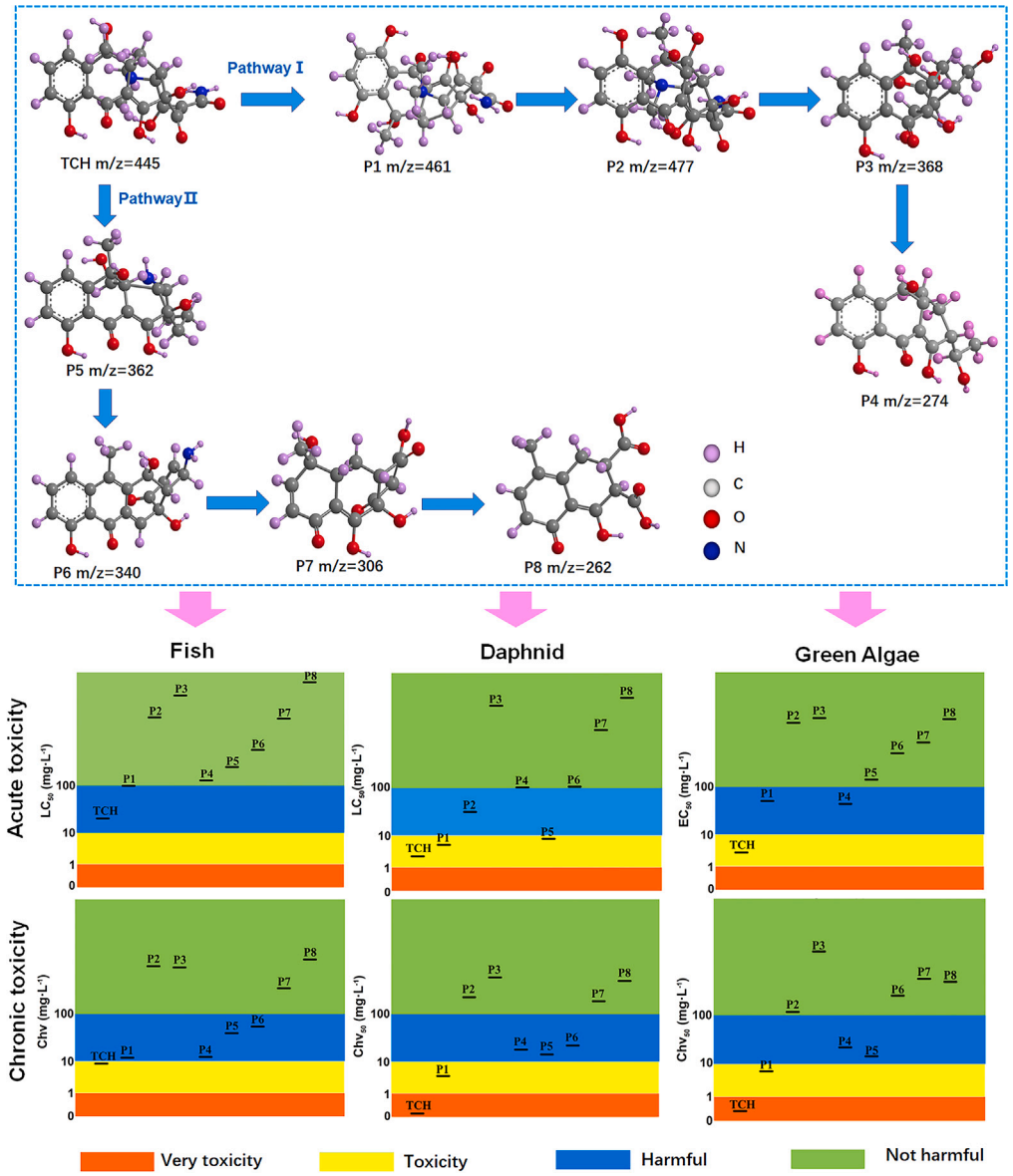

Figure 8. The pathways of TCH degradation in the CoFe-LDH/MoS_2 system and toxicity evolution throughout the degradation process

Degradation pathways of TCH intermediate products and their toxicities

Possible degradation pathways of TCH

Under the influence of ROS, we identified eight degradation intermediates of TCH through HPLC-mass spectrometry at different reaction times. The comprehensive details regarding these intermediates, including their molecular weights and structures, were listed in Figures 8, S8, and S9. Tentative degradation pathways for TCH were proposed and illustrated in Figure 8. We proposed two possible degradation pathways for TCH (m/z = 445), which is known to contain amine group, phenolic group, and double bond that are susceptible to attack by reactive species.[15,37] In pathway I, the double bond was attacked by ROS to yield the intermediate P1 (m/z = 461), followed by hydroxylation to generate the intermediate P2 (m/z = 477).[38,39] Subsequently, the intermediates P3 (m/z = 368) and P4 (m/z = 274) were generated through deamination, carboxylation, and ring-opening.[40,41] In pathway II, P5 (m/z = 362) was generated through the elimination of the amide group facilitated by TCH and subsequent removal of the methyl group in the -$N(CH_3)_2$. This was followed by deamination and ring-opening, resulting in the formation of P6 (m/z = 340) and P7 (m/z = 306).[42] Subsequently, intermediates P8 (m/z = 262) were generated through a series of ring-opening, dehydration, and carboxylation reactions.[6,15] Eventually, these intermediate products from all pathways underwent continuous degradation into smaller molecules and subsequent mineralization into CO_2 and H_2O. Additionally, Figure S10 demonstrated that the rate of TOC mineralization reached 76.6% within 60 min, indicating that most intermediates were eventually oxidized and degraded to H_2O, CO_2, and inorganic ions.

Toxicity assessments

Simultaneously, the toxicity of TCH and its degradation products to daphnia, fish, and green algae were predicted using the ECOSAR (2.0) software. The results were classified according to the Globally Harmonized Standard for the Classification of Chemicals (Table S3), as depicted in Figure 8.[43,44] The acute toxicity was estimated using LC50 for fish and daphnia, as well as EC50 for green algae; chronic toxicity was indicated by corresponding chronic toxicity value (ChV). The initial partial intermediates (such as P1) exhibited higher toxicity, whereas the low molecular weight intermediates (P7 and P8) demonstrated significantly reduced toxicity as degradation progressed, consistent with previous findings.[7,45] Upon prolonged reaction time, these intermediates underwent further decomposition and conversion into carbon dioxide and water, thereby eliminating their potential toxic effects. Consequently, the CoFe-LDH/MoS_2 system developed in this study also proved effective in detoxifying TCH.

Conclusion

In conclusion, the CoFe-LDH/MoS_2 heterojunction catalyst was synthesized through simple electrostatic interactions to facilitate Fenton degradation of organic pollutants. The ultrathin CoFe-LDH and MoS_2 layers in the heterostructure establish a robust interfacial contact, leading to an abundance of exposed Mo^{6+} sites that significantly enhance the degradation rate by promoting Fe^{3+}/Fe^{2+} cycling and facilitating rapid electron transfer. The developed CoFe-LDH/MoS_2+H_2O_2 system exhibited exceptional performance in the degradation of TCH (>85%) within 60 min across a wide pH range from acidic to basic (3−11). Benefiting from its heterostructure and low metal leaching rate, the CoFe-LDH/MoS_2 heterojunction catalyst exhibited superior cycling performance, with the TCH degradation rate still exceeding 90% after 10 cycles. Through quenching tests and EPR analysis, it was determined that the CoFe-LDH/MoS_2+H_2O_2 system effectively degraded TCH by generating •OH and $^1O_2$, with $^1O_2$ playing a crucial role. Additionally, based on HPLC-MS analysis of degradation intermediates, a reasonable assumption can be made regarding the degradation pathway of TCH. Furthermore, the ECOSAR assessment revealed that the intermediate product of TCH eventually transformed into a low-toxic compound composed of tiny molecules. Consequently, this study effectively addresses the bottlenecks in the Fenton reaction and will serve as a fundamental basis for developing novel catalyst systems for future organic pollutant degradation.

Limitations of the study

The developed CoFe-LDH/MoS_2+H_2O_2 system exhibited superior performance in the degradation of tetracycline (TCH) (>85%) within 60 min across a wide pH range from acidic to basic (3−11). In addition, the influence of anions on the degradation system was also tested. However, significant progress still needs to be made in order to achieve the actual degradation of wastewater, and it is imperative to conduct degradation tests using real wastewater samples.

STAR★METHODS

Detailed methods are provided in the online version of this paper and include the following:

- KEY RESOURCES TABLE
- RESOURCE AVAILABILITY
  - Lead contact
  - Materials availability
  - Data and code availability
- EXPERIMENTAL MODEL AND STUDY PARTICIPANT DETAILS
- METHOD DETAILS
  - The synthesis of ultrathin CoFe-LDH nanosheet
  - The synthesis of MoS_2 nanosheet
  - The synthesis of CoFe-LDH/MoS_2 nanocomposite
  - Degradation experiments
  - Characterization of catalysts
  - Toxicity evaluation
- QUANTIFICATION AND STATISTICAL ANALYSIS
- ADDITIONAL RESOURCES

SUPPLEMENTAL INFORMATION

Supplemental information can be found online at https://doi.org/10.1016/j.isci.2024.108996.

ACKNOWLEDGMENTS

This work was funded by Science and Technology innovation support program of Beijing University of Agriculture (BUA-HHXD2023010), China.

AUTHOR CONTRIBUTIONS

G.W. and Z.Y.F. conceived and developed this study. W.M., L.X.Y., S.Y.R., and W.J.G. performed the experiments and analyzed the data. S.T. and X.X. carried out BET measurements and toxicity assessments and drew the scheme images. F.F.Y. carried out SEM and HRTEM and drew the scheme images. The manuscript was written and polished by G.W. and W.M. All authors have read and agreed to the published version of the manuscript.

DECLARATION OF INTERESTS

The authors declare that they have no conflict of interest.

Received: August 30, 2023
Revised: December 6, 2023
Accepted: January 19, 2024
Published: January 26, 2024

REFERENCES

1. Ji, J., Yan, Q., Yin, P., Mine, S., Matsuoka, M., and Xing, M. (2021). Defects on CoS_{2-x}: Tuning Redox Reactions for Sustainable Degradation of Organic Pollutants. Angew. Chem. Int. Ed. *60*, 2903–2908. https://doi.org/10.1002/anie.202013015.
2. Shen, M., Huang, Z., Luo, X., Ma, Y., Chen, C., Chen, X., and Cui, L. (2020). Activation of persulfate for tetracycline degradation using the catalyst regenerated from Fenton sludge containing heavy metal: Synergistic effect of Cu for catalysis. Chem. Eng. J. *396*, 125238. https://doi.org/10.1016/j.cej.2020.125238.
3. Wang, W., Zhang, H., Chen, Y., and Shi, H. (2022). Efficient Degradation of Tetracycline via Coupling of Photocatalysis and Photo-Fenton Processes over a 2D/2D α-Fe_2O_3/g-C_3N_4 S-scheme Heterojunction Catalyst. Acta Phys. Chim. Sin. *38*, 2201008. https://www.whxb.pku.edu.cn/EN/10.3866/PKU.WHXB202201008.
4. Chen, R., Xia, J., Chen, Y., and Shi, H. (2022). S-Scheme-Enhanced PMS Activation for Rapidly Degrading Tetracycline Using $CuWO_{4-x}$/$Bi_{12}O_{17}Cl_2$ Heterostructures. Acta Phys. Chim. Sin. *39*, 2209012. https://www.whxb.pku.edu.cn/EN/10.3866/PKU.WHXB202209012.
5. Li, X., Liu, C., Chen, Y., Huang, H., and Ren, T. (2018). Antibiotic residues in liquid manure from swine feedlot and their effects on nearby groundwater in regions of North China. Environ. Sci. Pollut. R. *25*, 11565–11575. https://doi.org/10.1007/s11356-018-1339-1.
6. Zhang, Z., Wang, Z., Tan, J., Zhou, K., Garcia-Meza, J.V., Song, S., and Xia, L. (2023). Yeast-derived biochar to load $CoFe_2O_4$: Degradation of tetracycline hydrochloride by heterogeneous activation of peroxymonosulfate. J. Environ. Chem. Eng. *11*, 110020. https://doi.org/10.1016/j.jece.2023.110020.
7. Xiong, H., Zou, D., Zhou, D., Dong, S., Wang, J., and Rittmann, B.E. (2017). Enhancing degradation and mineralization of tetracycline using intimately coupled photocatalysis and biodegradation (ICPB). Chem. Eng. J. *316*, 7–14. https://doi.org/10.1016/j.cej.2017.01.083.
8. Liu, J., Lin, H., Dong, Y., He, Y., Liu, W., and Shi, Y. (2021). The effective adsorption of tetracycline onto MoS_2@Zeolite-5: Adsorption behavior and interfacial mechanism. J. Environ. Chem. Eng. *9*, 105912. https://doi.org/10.1016/j.jece.2021.105912.
9. Zhao, X., Wu, C., Dai, D., Ren, J., Li, T., and Ling, S. (2023). Silk nanofibrils-MOF composite membranes for pollutant removal from water. iScience *26*, 107290. https://doi.org/10.1016/j.isci.2023.107290.
10. Ren, L., Ma, J., Chen, M., Qiao, Y., Dai, R., Li, X., and Wang, Z. (2022). Recent advances in electrocatalytic membrane for the removal of micropollutants from water and wastewater. iScience *25*, 104342. https://doi.org/10.1016/j.isci.2022.104342.
11. Cheng, H., Huang, C., Wang, P., Ling, D., Zheng, X., Xu, H., Feng, C., Liu, H., Cheng, M., and Liu, Z. (2023). Molybdenum disulfide co-catalysis boosting nanoscale zero-valent iron based Fenton-like process: Performance and mechanism. Environ. Res. *227*, 115752. https://doi.org/10.1016/j.envres.2023.115752.
12. Cheng, H., Li, X., Huang, C., Zhu, J., Wang, P., Cao, H., Feng, C., Ling, D., Liu, H., and Cheng, M. (2023). Accelerated Fe(III)/Fe(II) cycle for rapid elimination of Rhodamine B by a novel Mo_2C co-catalytic Fe^{2+}/H_2O_2 system. J. Clean. Prod. *393*, 136354. https://doi.org/10.1016/j.jclepro.2023.136354.
13. Zhang, S., Song, S., Gu, P., Ma, R., Wei, D., Zhao, G., Wen, T., Jehan, R., Hu, B., and Wang, X. (2019). Visible-light-driven activation of persulfate over cyano and hydroxyl group co-modified mesoporous g-C_3N_4 for boosting bisphenol A degradation. J. Mater. Chem. A *7*, 5552–5560. https://doi.org/10.1039/C9TA00339H.
14. Han, T., Shi, H., and Chen, Y. (2024). Facet-dependent CuO/{010}$BiVO_4$ S-scheme photocatalyst enhanced peroxymonosulfate activation for efficient norfloxacin removal. J. Mater. Sci. Technol. *174*, 30–43. https://doi.org/10.1016/j.jmst.2023.03.053.
15. Xu, M., Wei, J., Chen, X., Pan, G., Li, J., Xing, L., Zhang, Y., Li, Y., Wang, Z., and Li, J. (2022). Satisfactory degradation of tetracycline by a pH-universal MnFe-LDH@BC cathode in electric Fenton process: Performances, mechanisms and toxicity assessments. J. Environ. Chem. Eng. *10*, 108409. https://doi.org/10.1016/j.jece.2022.108409.
16. Manjuri Bhuyan, P., Borah, S., Kumar Bhuyan, B., Hazarika, S., Gogoi, N., Gogoi, A., and Gogoi, P. (2023). Fe_3S_4/biochar catalysed heterogeneous Fenton oxidation of organic contaminants: Hydrogen peroxide activation and biochar enhanced reduction of Fe (III) to Fe (II). Sep. Purif. Technol. *312*, 123387. https://doi.org/10.1016/j.seppur.2023.123387.
17. Sun, Y., Zhou, P., Zhang, P., Meng, S., Zhou, C., Liu, Y., Zhang, H., Xiong, Z., Duan, X., and Lai, B. (2022). New insight into carbon materials enhanced Fenton oxidation: A strategy for green iron(III)/iron(II) cycles. Chem. Eng. J. *450*, 138423. https://doi.org/10.1016/j.cej.2022.138423.
18. Guo, R., Zhu, Y., Cheng, X., Li, J., and Crittenden, J.C. (2020). Efficient degradation of lomefloxacin by Co-Cu-LDH activating peroxymonosulfate process: Optimization, dynamics, degradation pathway and mechanism. J. Hazard Mater. *399*, 122966. https://doi.org/10.1016/j.jhazmat.2020.122966.
19. Ran, X., Sun, T., Zhou, R., Wei, C., Gao, W., and Zhao, H. (2023). In situ formation of Cu_2O decorated CuZnAl-layered double hydroxide heterostructured photocatalysts for enhancing the degradation of tetracycline under visible light. New J. Chem. *47*, 2914–2923. https://doi.org/10.1039/D2NJ04564H.
20. Lu, H., Zhu, Z., Zhang, H., Zhu, J., Qiu, Y., Zhu, L., and Küppers, S. (2016). Fenton-Like Catalysis and Oxidation/Adsorption Performances of Acetaminophen and Arsenic Pollutants in Water on a Multimetal Cu–Zn–Fe-LDH. ACS Appl. Mater. Inter. *8*, 25343–25352. https://doi.org/10.1021/acsami.6b08933.
21. Zhang, H., Li, G., Deng, L., Zeng, H., and Shi, Z. (2019). Heterogeneous activation of hydrogen peroxide by cysteine intercalated layered double hydroxide for degradation of organic pollutants: Performance and mechanism. J. Colloid Interface Sci. *543*, 183–191. https://doi.org/10.1016/j.jcis.2019.02.059.
22. Yang, Y., Wang, Q., Aleisa, R., Zhao, T., Ma, S., Zhang, G., Yao, T., and Yin, Y. (2021). MoS_2/FeS Nanocomposite Catalyst for Efficient Fenton Reaction. ACS Appl. Mater. Inter. *13*, 51829–51838. https://doi.org/10.1021/acsami.1c02864.
23. Zhao, Q., Zhou, W., Zhang, M., Wang, Y., Duan, Z., Tan, C., Liu, B., Ouyang, F., Yuan, Z., Tai, H., and Jiang, Y. (2022). Edge-Enriched $Mo_2TiC_2T_x$/MoS_2 Heterostructure with Coupling Interface for Selective NO_2 Monitoring. Adv. Funct. Mater. *32*, 2203528. https://doi.org/10.1002/adfm.202203528.
24. Xing, M., Xu, W., Dong, C., Bai, Y., Zeng, J., Zhou, Y., Zhang, J., and Yin, Y. (2018). Metal

Sulfides as Excellent Co-catalysts for H_2O_2 Decomposition in Advanced Oxidation Processes. Chem *4*, 1359–1372. https://doi.org/10.1016/j.chempr.2018.03.002.

25. Zhu, L., Ji, J., Liu, J., Mine, S., Matsuoka, M., Zhang, J., and Xing, M. (2020). Designing 3D-MoS_2 Sponge as Excellent Cocatalysts in Advanced Oxidation Processes for Pollutant Control. Angew. Chem. Int. Ed. *59*, 13968–13976. https://doi.org/10.1002/anie.202006059.
26. Qiu, C., Hao, X., Tan, L., Wang, X., Cao, W., Liu, J., Zhao, Y., and Song, Y.F. (2020). 500 nm induced tunable syngas synthesis from CO_2 photoreduction by controlling heterojunction concentration. Chem. Commun. *56*, 5354–5357. https://doi.org/10.1039/D0CC00971G.
27. Yang, J.-C.E., Lin, Y., Peng, H.-H., Yuan, B., Dionysiou, D.D., Huang, X.-D., Zhang, D.-D., and Fu, M.-L. (2020). Novel magnetic rod-like Mn-Fe oxycarbide toward peroxymonosulfate activation for efficient oxidation of butyl paraben: Radical oxidation versus singlet oxygenation. Appl. Catal. B Environ. *268*, 118549. https://doi.org/10.1016/j.apcatb.2019.118549.
28. Ding, D., Liu, C., Ji, Y., Yang, Q., Chen, L., Jiang, C., and Cai, T. (2017). Mechanism insight of degradation of norfloxacin by magnetite nanoparticles activated persulfate: Identification of radicals and degradation pathway. Chem. Eng. J. *308*, 330–339. https://doi.org/10.1016/j.cej.2016.09.077.
29. Wu, T., Li, X., Weng, C.-H., Ding, F., Tan, F., and Duan, R. (2023). Highly efficient $LaMO_3$ (M = Co, Fe) perovskites catalyzed Fenton's reaction for degradation of direct blue 86. Environ. Res. *227*, 115756. https://doi.org/10.1016/j.envres.2023.115756.
30. Yan, Q., Lian, C., Huang, K., Liang, L., Yu, H., Yin, P., Zhang, J., and Xing, M. (2021). Constructing an Acidic Microenvironment by MoS_2 in Heterogeneous Fenton Reaction for Pollutant Control. Angew. Chem. Int. Ed. Engl. *60*, 17155–17163. https://doi.org/10.1002/anie.202105736.
31. He, Z., Chen, M., Xu, M., Zhou, Y., Zhang, Y., and Hu, G. (2023). $LaCo_{0.5}Ni_{0.5}O_3$ perovskite for efficient sulfafurazole degradation via peroxymonosulfate activation: Catalytic mechanism of interfacial structure. Appl. Catal. B Environ. *335*, 122883. https://doi.org/10.1016/j.apcatb.2023.122883.
32. Chen, K., Yang, X., Hao, R., Shao, M., Yang, X., Li, X., Li, Y., Liu, J., and Zhang, S. (2023). Optimized Cu_2O-{100} facet for generation of different reactive oxidative species via peroxymonosulfate activation at specific pH values to efficient acetaminophen removal. Nanotechnol. Rev. *12*, 20220542. https://doi.org/10.1515/ntrev.2022.0542.
33. Huang, C., Liu, H., Sun, C., Wang, P., Tian, Z., Cheng, H., Huang, S., Yang, X., Wang, M., and Liu, Z. (2023). Peroxymonosulfate activation by graphene oxide-supported 3D-MoS_2/$FeCo_2O_4$ sponge for highly efficient organic pollutants degradation. Environ. Pollut. *325*, 121391. https://doi.org/10.1016/j.envpol.2023.121391.
34. Zhang, J., Wang, Y., Hong, M., Peng, B., Bao, C., Xu, X., Li, D., Chen, J., Wang, B., and Zhang, Q. (2023). Ferrocene-based resin as heterogeneous fenton-like catalyst for efficient treatment of high salinity wastewater at acidic, neutral, and basic pH. Chem. Eng. J. *464*, 142450. https://doi.org/10.1016/j.cej.2023.142450.
35. Yi, Q., Ji, J., Shen, B., Dong, C., Liu, J., Zhang, J., and Xing, M. (2019). Singlet Oxygen Triggered by Superoxide Radicals in a Molybdenum Cocatalytic Fenton Reaction with Enhanced REDOX Activity in the Environment. Environ. Sci. Technol. *53*, 9725–9733. https://doi.org/10.1021/acs.est.9b01676.
36. Yang, Y., Zhen, W., Zhao, T., Wu, M., Ma, S., Zhao, L., Wu, J., Liu, L., Zhang, J., and Yao, T. (2023). Engineering low-valence $Mo^{\delta+}$ ($0<\delta<4$) sites on MoS_2 surface: Accelerating Fe^{3+}/Fe^{2+} cycle, maximizing H_2O_2 activation efficiency, and extending applicable pH range in photo-Fenton reaction. J. Clean. Prod. *404*, 136918. https://doi.org/10.1016/j.jclepro.2023.136918.
37. Zhang, N., Chen, J., Fang, Z., and Tsang, E.P. (2019). Ceria accelerated nanoscale zerovalent iron assisted heterogenous Fenton oxidation of tetracycline. Chem. Eng. J. *369*, 588–599. https://doi.org/10.1016/j.cej.2019.03.112.
38. Huang, Z., and Liu, H. (2023). Insights into the pathways, intermediates, influence factors and toxicological properties in the degradation of tetracycline by TiO_2-based photocatalysts. J. Environ. Chem. Eng. *11*, 110587. https://doi.org/10.1016/j.jece.2023.110587.
39. Zhang, Q., Jiang, L., Wang, J., Zhu, Y., Pu, Y., and Dai, W. (2020). Photocatalytic degradation of tetracycline antibiotics using three-dimensional network structure perylene diimide supramolecular organic photocatalyst under visible-light irradiation. Appl. Catal., B *277*, 119122. https://doi.org/10.1016/j.apcatb.2020.119122.
40. Guo, H., Niu, C.-G., Zhang, L., Wen, X.-J., Liang, C., Zhang, X.-G., Guan, D.-L., Tang, N., and Zeng, G.-M. (2018). Construction of Direct Z-Scheme AgI/$Bi_2Sn_2O_7$ Nanojunction System with Enhanced Photocatalytic Activity: Accelerated Interfacial Charge Transfer Induced Efficient Cr(VI) Reduction, Tetracycline Degradation and Escherichia coli Inactivation. ACS Sustain. Chem. Eng. *6*, 8003–8018. https://doi.org/10.1021/acssuschemeng.8b01448.
41. Cao, J., Lai, L., Lai, B., Yao, G., Chen, X., and Song, L. (2019). Degradation of tetracycline by peroxymonosulfate activated with zero-valent iron: Performance, intermediates, toxicity and mechanism. Chem. Eng. J. *364*, 45–56. https://doi.org/10.1016/j.cej.2019.01.113.
42. Huang, L., Bao, D., Li, J., Jiang, X., and Sun, X. (2021). Construction of Au modified direct Z-scheme g-C_3N_4/defective ZnO heterostructure with stable high-performance for tetracycline degradation. Appl. Surf. Sci. *555*, 149696. https://doi.org/10.1016/j.apsusc.2021.149696.
43. McGregor, D., Boobis, A., Binaglia, M., Botham, P., Hoffstadt, L., Hubbard, S., Petry, T., Riley, A., Schwartz, D., and Hennes, C. (2010). Guidance for the classification of carcinogens under the Globally Harmonised System of Classification and Labelling of Chemicals (GHS). Crit. Rev. Toxicol. *40*, 245–285. https://doi.org/10.3109/10408440903384717.
44. Chen, R., Zhang, H., Dong, Y., and Shi, H. (2024). Dual metal ions/BNQDs boost PMS activation over copper tungstate photocatalyst for antibiotic removal: Intermediate, toxicity assessment and mechanism. J. Mater. Sci. Technol. *170*, 11–24. https://doi.org/10.1016/j.jmst.2023.07.005.
45. Darvishi Cheshmeh Soltani, R., Naderi, M., Boczkaj, G., Jorfi, S., and Khataee, A. (2021). Hybrid metal and non-metal activation of Oxone by magnetite nanostructures co-immobilized with nano-carbon black to degrade tetracycline: Fenton and electrochemical enhancement with bio-assay. Sep. Purif. Technol. *274*, 119055. https://doi.org/10.1016/j.seppur.2021.119055.
46. Xie, J., Zhang, J., Li, S., Grote, F., Zhang, X., Zhang, H., Wang, R., Lei, Y., Pan, B., and Xie, Y. (2013). Controllable Disorder Engineering in Oxygen-Incorporated MoS_2 Ultrathin Nanosheets for Efficient Hydrogen Evolution. J. Am. Chem. Soc. *135*, 17881–17888. https://doi.org/10.1021/ja408329.
47. Dong, Y.D., Zhang, L.Q., Zhou, P., Liu, Y., Lin, H., Zhong, G.J., Yao, G., Li, Z.M., and Lai, B. (2022). Natural cellulose supported carbon nanotubes and Fe_3O_4 NPs as the efficient peroxydisulfate activator for the removal of bisphenol A: An enhanced non-radical oxidation process. J. Hazard Mater. *423*, 127054. https://doi.org/10.1016/j.jhazmat.2021.127054.

STAR★METHODS

KEY RESOURCES TABLE

REAGENT or RESOURCE	SOURCE	IDENTIFIER
Chemicals, peptides, and recombinant proteins		
$Co(NO_3)_2 \cdot 6H_2O$	Aladdin, China	13478-00-7
$Fe(NO_3)_3 \cdot 9H_2O$	Aladdin, China	7782-61-8
Na_2CO_3	Aladdin, China	497-19-8
$NaHCO_3$	Aladdin, China	144-55-8
NaOH	Aladdin, China	1310-73-2
$(NH_4)_6Mo_7O_{24} \cdot 4H_2O$	Aladdin, China	12054-85-2
thiourea	InnoChem, China	62-56-6
H_2O_2	InnoChem, China	7722-84-1
HCl	InnoChem, China	7647-01-0
NaCl	Aladdin, China	7647-14-5
$NaNO_3$	InnoChem, China	7631-99-4
NaH_2PO_4	Aladdin, China	7558-79-4
tert-butanol (TBA)	InnoChem, China	75-65-0
p-benzoquinone (*p*-BQ)	InnoChem, China	106-51-4
furfuryl alcohol (FFA)	InnoChem, China	98-00-0
5,5-dimethyl-1-pyrroline-1-oxide (DMPO)	InnoChem, China	3317-61-1
2,2,6,6-tetramethyl-4-piperidone (TEMP)	InnoChem, China	826-36-8
tetracycline hydrochloride (TCH)	InnoChem, China	64-75-5
rhodamine B (RhB)	InnoChem, China	81-88-9
methyl orange (MO)	InnoChem, China	547-58-0
phenol	InnoChem, China	108-95-2

RESOURCE AVAILABILITY

Lead contact

Further information and requests for resources and reagents should be directed to and will be fulfilled by the lead contact, Wa Gao (gaowa@bua.edu.cn).

Materials availability

Catalysts are available up on request.

Data and code availability

Data reported in this article will be shared by the lead contact on request.

This paper does not report original codes.

Any additional information required to reanalyze the data reported in this paper is available from the lead contact upon request.

EXPERIMENTAL MODEL AND STUDY PARTICIPANT DETAILS

This study does not use experimental models.

METHOD DETAILS

The synthesis of ultrathin CoFe-LDH nanosheet

The formation process of ultrathin CoFe-LDH nanosheet was illustrated in Figure 1 (Step 1). Typically, it involved the double drop co-precipitation of salt (n ($Co(NO_3)_2 \cdot 6H_2O$)/n($Fe(NO_3)_3 \cdot 9H_2O$) = 4:1) in a 40 mL aqueous solution and an alkali solution prepared by dissolving 2.732 g NaOH and 2.258 g Na_2CO_3 in 40 mL aqueous solution. Subsequently, the above two solutions were slowly dropped into 40 mL of deionized water simultaneously and vigorously stirred. The pH was maintained at approximately 8.5 through magnetic stirring at room temperature.[26] Following centrifugation and water washing, a brown-colored sample was obtained. Finally, the resulting pellet was dried overnight in an oven set at 60°C.

The synthesis of MoS_2 nanosheet

The formation process of MoS_2 was schematically illustrated in Figure 1 (Step 2). Briefly, MoS_2 was synthesized via the hydrothermal method at 180°C for 24 h using ammonium heptamolybdate and thiourea as precursors dissolved in 45 mL deionized water.[46] After centrifuging and washing with water and ethanol, the dark gray sample was collected.

The synthesis of CoFe-LDH/MoS_2 nanocomposite

The formation process of CoFe-LDH/MoS_2 nanocomposite was schematically illustrated in Figure 1 (Step 3). CoFe-LDH and MoS_2, with the mass fraction of 90% and 10% respectively, were dissolved in aqueous solution by gradually adding the MoS_2 nanosheet suspension to the CoFe-LDH suspension while stirring magnetically for 48 h. The positively charged CoFe-LDH nanosheet and the negatively charged MoS_2 nanosheet were electrostatically self-assembled in aqueous solution to obtain CoFe-LDH/MoS_2 nanocomposite.[26] The color of the solution gradually changed from brown to dark gray. Finally, after low-speed centrifugation, the supernatant became transparent, indicating successful synthesis of the nanocomposite. The CoFe-LDH/MoS_2 nanomaterials with varying proportions were synthesized using the aforementioned methods, with MoS_2 mass percentages of 2%, 4%, 6%, 8%, 10%, 20% and 30%.

Degradation experiments

All degradation experiments were carried out in 500 mL beaker at 25°C (±2°C). In a typical process, 30 mg of catalyst was added to a solution of 200 mL with a concentration of TCH at 50 mg L^{-1}. Subsequently, the above mixture was magnetically stirred in the dark for 0.5 h to achieve the adsorption/desorption equilibrium, followed by the addition of 80 mmol L^{-1} H_2O_2 (30%) and illuminated for 1.5 h. At specific time intervals, a syringe was used to draw out 4 mL of the suspension every 15 min, and then the supernatant was obtained by filtering it through a microporous filter with a pore size of 0.22 mm. The concentrations of TCH were determined using both UV-vis spectrometer (Shimadzu, UV-3600, Japan) and HPLC-MS (Shimadzu, LC-6AD, Japan). The degradation efficiency was calculated using the following formula:

$$\text{Degradation efficiency } \% = (1 - C_t / C_0) \times 100\% \quad \text{(Equation 12)}$$

where C_0 and C_t are the concentrations of TCH at irradiation time zero and any irradiation time, respectively.

The degradation experiment mentioned above was carried out three times in each group. The average result of the three repeated experiments was considered as the final outcome, and the error bar in the figure represents the estimation of error. To identify the primary reactive species generated during the catalytic process, corresponding free radical scavengers were introduced into the TCH solution. FFA, TBA and p-BQ were used as the scavengers for $^1O_2$, •OH, and $•O_2^-$, respectively. In a typical experiment, 30 mg CoFe-LDH/MoS_2 was added to 100 mL TCH solution (100 mg/L), followed by adding different concentrations of FFA (20, 30, 40 and 50 mmol/L), TBA (50, 100, 200 and 300 mol/L) and *p*-BQ (2, 5, 10 and 15 mmol/L) as the quenching agents.[27,34,47] The possible TCH degradation intermediates were ascertained by an HPLC-MS. The mineralization rate of TCH after the reaction was analyzed by a total organic carbon analyzer (TOC, Shimadzu TOC-L, Japan).

Characterization of catalysts

The crystallinities of CoFe-LDH, MoS_2, and CoFe-LDH/MoS_2 were determined using X-ray powder diffractometry (XRD). Powder XRD measurements were performed on a Rigaku XRD- 6000 diffractometer with Cu K_a radiation (λ = 0.15418 nm) at 40 kV and 40 mA. The scanning rate was set at 5° min^{-1}, and the 2θ angle ranged from 5° to 80°. The morphology of the CoFe-LDH/MoS_2 catalyst was investigated using a scanning electron microscope (SEM, Zeiss Sigma 300, Germany) and high resolution transmission electron microscope (HRTEM, FEI Tecnai G2 F30, USA). The specific surface areas of the samples were recorded by the Brunner–Emmett–Teller (BET) technique (ASAP2460, USA). The catalyst surface's functional groups were identified using Fourier transform infrared spectroscopy (FT-IR, Thermo Scientific, Nicolet iS5, USA). X-ray photoelectron spectroscopy (XPS) information was obtained using a spectrometer (Thermo Escalab 250Xi, USA). The reactive oxygen species were monitored by electron paramagnetic resonance (EPR, Bruker EMX Plus, USA) spectrometer, and DMPO and TEMP were used as a trap for $·O_2^-$, ·OH and $^1O_2$. Furthermore, HPLC-MS (Shimadzu, LC-6AD, Japan) equipped with a Waters XTerra C18 column was used to investigate the intermediates during the degradation of TCH and its possible degradation pathways.

Toxicity evaluation

Biological toxicity tests were also conducted on the aqueous solution of tetracycline hydrochloride before and after degradation, using deionized water as well as the pre-degradation and post-degradation solutions of tetracycline hydrochloride for mung beans cultivation. By comparing the length and thickness of mung beans, we assessed the degradation effect and biological toxicity of TCH.

QUANTIFICATION AND STATISTICAL ANALYSIS

This study does not include statistical analysis or quantification.

ADDITIONAL RESOURCES

This work does not include any additional resource.